Atmospheric Pollution Research 8 (2017) 900–911

Contents lists available at ScienceDirect

Atmospheric Pollution Research

journal homepage: http://www.journals.elsevier.com/locate/apr

Characteristics and origins of air pollutants and carbonaceous aerosols during wintertime haze episodes at a rural site in the Yangtze River Delta, China

Mengying Bao [a, b, c, d], Fang Cao [a, b, c, d], Yunhua Chang [a, b, c, d], Yan-Lin Zhang [a, b, c, d, *], Yaqi Gao [a, b, c, d], Xiaoyan Liu [a, b, c, d], Yuanyuan Zhang [a, b, c, d], Wenqi Zhang [a, b, c, d], Tianran Tang [a, b, c, d], Zufei Xu [a, b, c, d], Shoudong Liu [a, b, c, d], Xuhui Lee [a, b, c, d], Jun Li [e], Gan Zhang [e]

[a] Key Laboratory of Meteorological Disaster Ministry of Education (KLME), Nanjing 210044, China
[b] Joint International Research Laboratory of Climate and Environment Change (ILCEC), Nanjing 210044, China
[c] Collaborative Innovation Center on Forecast and Evaluation of Meteorological Disasters (CIC-FEMD), Nanjing 210044, China
[d] Yale-NUIST Center on Atmospheric Environment, Nanjing University of Information Science and Technology, Nanjing 210044, China
[e] State Key Laboratory of Organic Geochemistry, Guangzhou Institute of Geochemistry, Chinese Academy of Sciences, Guangzhou 510640, China

ARTICLE INFO

Article history:
Received 17 December 2016
Received in revised form
6 March 2017
Accepted 6 March 2017
Available online 15 March 2017

Keywords:
Air pollution
$PM_{2.5}$
Carbonaceous aerosols
Back trajectories
Sources

ABSTRACT

China has frequently suffered regional-scale haze pollution in recent years. In this study, real-time observation data such as $PM_{2.5}$, PM_{10}, SO_2, NO_2, CO and O_3 were used to analyze wintertime haze events at a rural site (Dongshan) in the Yangtze River Delta (YRD). 3-hour resolution organic carbon (OC) and elemental carbon (EC) were also measured to further investigate the sources of $PM_{2.5}$. The hybrid receptor models were used to identify source regions of $PM_{2.5}$. The results showed that both regional transport and local emissions significantly contribute to air pollution at Dongshan during haze periods. The source areas affecting high $PM_{2.5}$ concentrations were mainly located in nearby urbanized provinces (i.e., Jiangsu, Anhui and Zhejiang) and industrial provinces (i.e., Shandong and Hebei) in eastern China. Furthermore, open biomass-burning emissions in south China (i.e., Jiangxi, Hunan, Guangdong and Fujian) decreased regional air quality, which was supported by MODIS fire spots and receptor models. During clean periods, air masses were originated from remote regions such as Mongolia and oceanic areas (i.e., the Yellow Sea and the East Sea). Enhanced secondary organic carbon (SOC) formation was found under long-range transport when OC aging was favorable. Contrarily, relatively low SOC formation was found when the site was dominated by local emissions. In addition to local emissions, high $PM_{2.5}$ concentrations at Dongshan were apparently affected by either regional or long-range transport, which were characterized by relatively low and high wind speeds, respectively. It is necessary to implement the emission control strategies for the industrial and urbanized areas.

1. Introduction

Due to the rapid economic growth and urbanization over the last few decades in China, air pollution and heavy haze have become a serious environmental issue and led to a global concern (Yu, 2014; Chan and Yao, 2008). Haze is defined as a weather phenomenon with low atmospheric visibility (less than 10 km) under the conditions of 80% relative humidity (Yu et al., 2014). Previous studies have shown that anthropogenic emissions and meteorological conditions are the two most important factors causing extreme haze pollution (Xu et al., 2015; Zhang et al., 2015a). Fine aerosols (particulate matter with aerodynamic diameters equivalent to or less than 2.5 μm; $PM_{2.5}$) have been reported to be an important determinant for the formation of regional haze events (Wang et al., 2014a; Yang et al., 2011; Cao et al., 2012). Gaseous species such as NO_2, SO_2 as well as volatile organic compounds can

* Corresponding author. Yale-NUIST Center on Atmospheric Environment, Nanjing University of Information Science and Technology, Nanjing 210044, China.
E-mail address: dryanlinzhang@outlook.com (Y.-L. Zhang).

Peer review under responsibility of Turkish National Committee for Air Pollution Research and Control.

http://dx.doi.org/10.1016/j.apr.2017.03.001
1309-1042/

react in the atmosphere and produce secondary PM pollution (Chang et al., 2011; Huang et al., 2014; Yu et al., 2007). High occurrence of haze has important impacts on visibility, air quality, climate change and human health (Yu et al., 2013, 2001, 2010; Chen et al., 2013). Coal combustion, biomass burning, traffic and industrial emissions are the main contributors of extreme haze pollution in China (Adame et al., 2012; Zhang et al., 2015c, 2015d; Cao et al., 2015).

Carbonaceous species, as significant chemical components of $PM_{2.5}$, have also been found to be widely associated with global radiative transfer, health problems and visibility deterioration (Ramanathan et al., 2007; Mcconnell et al., 2007; Cao et al., 2005). Carbonaceous aerosol is usually divided into organic carbon (OC) and elemental carbon (EC) fractions. EC is mainly emitted from fossil fuel and biomass combustion, and is of special interest because it could cause positive radiative forcing and was found to be the second most important factor of global warming behind CO_2 (Jacobson, 2001). OC originates both from direct emissions as primary organic carbon (POC) and gas-to-particle conversion as secondary organic carbon (SOC) and can cause negative forcing due to its scattering of sunlight (Cao et al., 2007; Mcconnell et al., 2007; Kaiser and Yun, 2002). The knowledge on carbonaceous aerosols is important for understanding the impacts of emissions on regional air quality and climate change.

There have been a large number of studies focusing on the physical and chemical characteristics (Yu and Zhang, 2011), formation mechanisms (Yu et al., 2008; Wang et al., 2014c; Guo et al., 2014; Yang et al., 2005), climate effect (Yu et al., 2013; Ramanathan et al., 2007) and source apportionments (Zhang et al., 2015c) of aerosol particles in China, especially in the high-populated city clusters such as the Beijing-Tianjin-Hebei (BTH) regions, the Yangtze River Delta (YRD) and the Pearl River Delta (PRD) (Wang, 2015; Cao et al., 2013; Tan et al., 2009). For example, Zhang and Cao (2015) investigated the spatial and seasonal distribution of $PM_{2.5}$ in 190 cities of China and found that high $PM_{2.5}$ level appears in the spring of the Northwest and West Central China, and autumn of the East China. The $PM_{2.5}$ concentrations were also found closely associated with variations of the boundary layer depth and human activities. Zhang et al. (2007a) investigated the characteristics of carbonaceous species in PM_{10} and trace gases in winter in Beijing and found strong correlation between OC, EC with PM_{10}, SO_2 and CO, indicating the similar source of them. Vehicle emission with low OC/EC ratio and coal combustion with high OC/EC ratio were the main sources for carbonaceous aerosols in winter in Beijing. Wang et al. (2015) discussed possible causes of a severe haze episode in the Yangtze River Delta. It was found that meteorological conditions played a very important role in the formation of haze. Strong relationship between PM_{10}, $PM_{2.5}$, SO_2, NO_2 and CO was found, indicating the great contributors of vehicular emissions and biomass burning for the haze episode. Most of these studies reported air pollution on the regional or national scale; however, only a few studies have been conducted at rural sites in China, especially on the transport characteristics of air pollutants between rural sites and surrounded urban areas.

Air pollution is not only a local but also a regional or even a global-scale problem (Wang et al., 2010). Some air pollutants can be transported over hundreds of or even thousands of kilometers. (Bergin et al., 2005). Back trajectory and cluster analysis as well as hybrid receptor models such as the potential source contribution function (PSCF) and the concentration weighted trajectory (CWT) methods have been widely used to assess the transport pathways and the source regions of air pollutants (Yu et al., 2014; Zhang et al., 2014, 2015b; Yan et al., 2015; Sadyś et al., 2014). For example, Yu et al. (2014) reported that the major contributions to air pollutants in Hangzhou were from the southeastern sources based on the back trajectories and receptor model analysis. Karaca et al. (2009) evaluated long-range source contributions to the PM_{10} profile of Istanbul, Turkey in 2008. Their results showed that air masses arriving at Istanbul were seasonally dependent and the potential source region of PM_{10} in Istanbul included Europe, Asia and the Mediterranean region. Kim et al. (2009) investigated transport patterns of air pollution in Korea and found that long-range or regional transport between heavily polluted urban and rural area can significantly affect the air pollution level in rural sites.

In this study we analyzed 6 major air pollutants (i.e., $PM_{2.5}$, PM_{10}, CO, SO_2, NO_2 and O_3) and carbonaceous species (i.e., OC and EC) in $PM_{2.5}$ from January 15 to 28, 2015, at Dongshan. The objectives of this study are 1) to investigate the temporal variations and characteristics of major air pollutants and the carbonaceous components in $PM_{2.5}$ during wintertime haze events; 2) to evaluate the impact of local and regional transport sources on the formation of haze episodes in Dongshan using the air mass back trajectory and hybrid receptor models (PSCF and CWT).

2. Measurement and methods

2.1. Sampling site and observational data

Our measurement site Dongshan (31.04°N, 120.26°E) is located on the southeast bank of the Taihu Lake in eastern China, a rural area of Suzhou, which is the fifth largest city in the Yangtze River Delta (YRD) region (see Fig. 1). Dongshan has an eastern Asian monsoon climate accompanying seasonally changing prevailing winds which is warm and humid with four clear seasons. Due to its unique topography and humid climate, Dongshan is very sensitive to regional transport of air masses from its surrounding industrial areas and population centers.

Hourly mass concentrations of $PM_{2.5}$ and PM_{10} were determined by the β-Ray method (BAM-1020, MetOne, America) at the Dongshan Automatic Meteorological Station (DAMS). Meanwhile, real-time hourly concentrations of gaseous species including SO_2, NO_2, CO and O_3 were measured using the ultraviolet fluorescence method, the chemiluminescence method, the gas filter correlation analysis method and the ultraviolet photometric method (EC9800 series, Ecotech, Australia), respectively. The instrumental operation maintenance, data assurance and quality control were performed according to the Chinese Ministry of Environmental Protection Standards for PM_{10}, $PM_{2.5}$ (MEP, 2013a) and for SO_2, NO_2, O_3 and CO (MEP, 2013b) (Zhang and Cao, 2015). The wind speed data were obtained from the DAMS.

2.2. Filter-based $PM_{2.5}$ sampling

The 3-h $PM_{2.5}$ samples were collected on prebaked quartz fiber filters (QFF, PALL, America) with 8 × 10 inches by a high volume air sampler (KC-1000, Laoshan, China) at a flow rate of 1.05 m^3 min^{-1} in the DAMS (31.04°N, 120.26°E) from January 15 to 28, 2015. A total of 99 samples were collected including two filed bank filters collected following 10 min exposures to ambient air without active sampling.

All QFFs were pre-baked at 450 °C for 6 h before sampling to remove carbon contaminations. Before and after sampling, all QFFs were weighed by electronic balance (Sartorius, 0.1 mg, Germany). To avoid the errors introduces by variations of room temperature and relative humidity, the filters were equilibrated at 25 ± 0.5 °C and 30 ± 5% relative humidity for 72 h before being weighed. After weighting, the filters were wrapped in aluminum foils, packed in sealable bags and stored at −20 °C for further analysis. All procedures during sampling and analysis were strictly quality

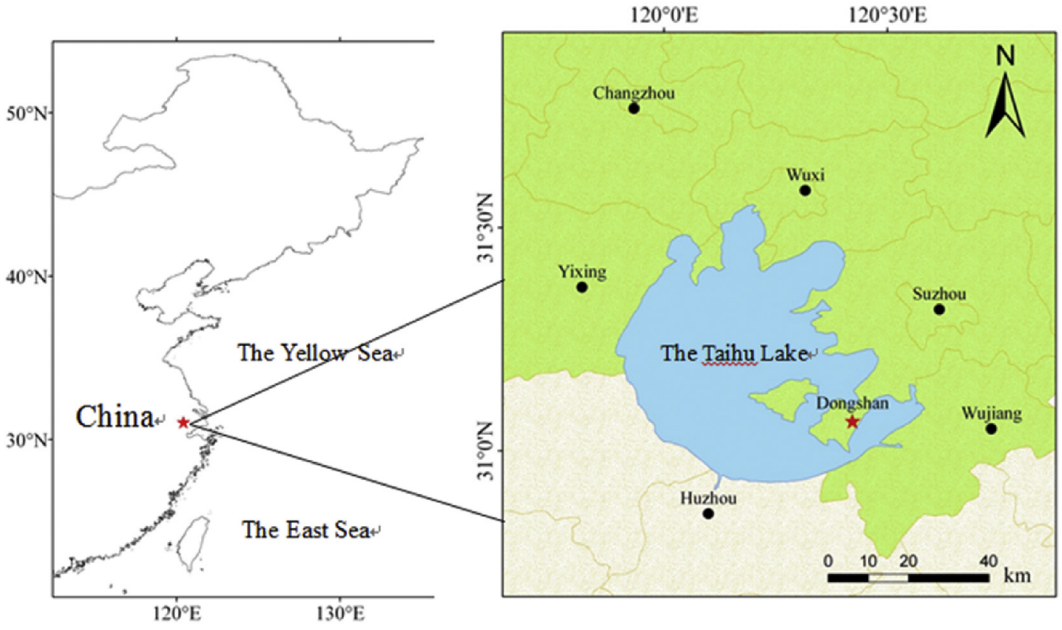

Fig. 1. Sampling location at Dongshan site in Jiangsu, China.

controlled to avoid any potential contamination.

2.3. Chemical analysis

The $PM_{2.5}$ samples were analyzed for OC and EC using a Desert Research Institute (DRI) Model 2001 Thermal Optical Carbon Analyzer (Atmoslytic Inc., Calabasas, USA). A 0.526 cm^2 punch from each QFF was analyzed following the IMPROVE thermal optical reflectance (TOR) protocol (Cao et al., 2007). For quality control, replicate analyses of 10% of the total samples yielded differences of less than 8% for OC and 10% for EC. The sample results were corrected by the blank values.

2.4. Back trajectories analysis

To evaluate the air mass origins of $PM_{2.5}$, 48-h back trajectories at Dongshan (31.04°N, 120.26°E) were calculated 8 times a day (0:00, 3:00, 6:00, 9:00, 12:00, 15:00, 18:00, 21:00 UTC) by using the Hybrid Single-Particle Lagrangian Integrated Trajectory (HYSLPIT4.8) model, provided by the National Oceanic and Atmospheric Administration (NOAA) (NOAA/ARL, 2007; Draxler and Hess, 1998). In order to investigate the behavior of the air masses circulation in the planetary boundary layer (PBL), these trajectories have been calculated to 500 m corresponding to the upper middle height of the PBL, representing well-mixed convective boundary layer for regional transport investigation (Xu and Akhtar, 2010). The National Center for Environmental Prediction Global Data Assimilation System (NCEP GDAS) data obtained from NOAA (GDAS, 2007) with a spatial resolution of 1° × 1° and 24 levels of vertical resolution were used as meteorological data input to the model.

2.5. PSCF and CWT models

The PSCF model can be used to localize the potential sources of aerosols at the receptor site (Hoh and Hites, 2004). For PSCF modeling, the region was divided into 0.5° × 0.5° grid. The PSCF value for a single grid cell is calculated by counting each trajectory segment endpoint that terminates within that grid cell (Ashbaugh et al., 1985) as follows:

$$PSCF_{ij} = \frac{m_{ij}}{n_{ij}} W_{ij} \tag{1}$$

where m_{ij} is the number of back-trajectory endpoints at the grid cell (i, j) corresponding to the measured concentrations of air pollutants higher than a given criterion value, which is set to the mean air pollutants concentrations during the haze pollution in this study. n_{ij} is the total number of endpoints falling in the grid cell. W_{ij} is an empirical weight function proposed by Zeng and Hopke (1989) to reduce the uncertainties of small n_{ij} on the PSCF values:

$$W_{ij} = \begin{cases} 1.0 & n_{ij} > 2Avg \\ 0.75 & Avg < n_{ij} < 2Avg \\ 0.5 & 0.5\,Avg < n_{ij} < Avg \\ 0.15 & 0 < n_{ij} < 0.5Avg \end{cases} \tag{2}$$

where Avg is the average number of trajectory segment endpoints in all cells.

The higher the PSCF value is, the higher possibility the areas have potential source of aerosols at the receptor site. It's difficult to separate moderate sources from strong ones for PSCF method because when pollutant concentrations are only slightly higher or extremely higher than the criterion, the grid cells will have the same PSCF value. To overcome the limitation, the CWT method was used to calculate the trajectory weighted concentration C_{ij} as follows (Hsu et al., 2003):

$$C_{ij} = \frac{\sum_{l=1}^{M} C_l T_{ijl}}{\sum_{l=1}^{M} T_{ijl}} W_{ij} \tag{3}$$

where l is the index of the trajectory, M is the total number of trajectories, C_l is the concentration measured on arrival of trajectory l, and T_{ij} is the time spent in the grid cell (i,j) by trajectory l. The higher the C_{ij} value is, the higher potential contributions to the high pollutant concentrations at the receptor site.

The trajectory cluster and receptor model analysis together with the geographic information system (GIS) visualization was performed with the software TrajStat (Wang et al., 2009). The TrajStat software

can identify the transport pathways and source regions by providing an integrated GIS interface to query, view and analyze trajectories and the corresponding measurement data at the receptor site.

3. Results and discussion

3.1. Characteristics of air pollutants and carbonaceous aerosols

3.1.1. Concentrations of major air pollutants

Concentrations of air pollutants ($PM_{2.5}$, PM_{10}, O_3, CO, SO_2 and NO_2) and $PM_{2.5}/PM_{10}$ ratio during January 15 to 28, 2015, at Dongshan are summarized in Table 1. The average concentrations of $PM_{2.5}$ and PM_{10} were 61.5 μg m^{-3} and 98.2 μg m^{-3} with the highest concentrations of 177.1 μg m^{-3} and 285.0 μg m^{-3}, respectively, which were 2.4 and 1.9 times of the corresponding Chinese National Ambient Air Quality Standards (NAAQS) of 75 μg m^{-3} and 150 μg m^{-3}, respectively (GB3095-2012). High concentrations of $PM_{2.5}$ and PM_{10} were observed at this rural area. The variation ranges of SO_2, NO_2, O_3 and CO concentrations were 5.4–186.0 μg m^{-3}, 12.2–238.8 μg m^{-3}, 10.7–129.7 μg m^{-3} and 0.1–3.1 mg m^{-3}, respectively, much lower than the hourly NAAQS for SO_2 (500 μg m^{-3}), NO_2 and O_3 (200 μg m^{-3}) and CO (10 mg m^{-3}), respectively. Compared with the data derived from the National Environment Monitoring Station, the air pollution level of Dongshan was relatively lower than the nearby high-populated cities such as Suzhou ($PM_{2.5}$, 101.9 μg m^{-3}; PM_{10}, 118.0 μg m^{-3}), Nanjing ($PM_{2.5}$, 110.8 μg m^{-3}; PM_{10}, 168.4 μg m^{-3}) and Wuxi ($PM_{2.5}$, 106.8 μg m^{-3}; PM_{10}, 152.2 μg m^{-3}), during the studied period. The mean $PM_{2.5}/PM_{10}$ was 62.8% with a range from 30.0% to 93.4%, indicating that fine particulate matter was a major fraction of PM_{10}.

The average mass concentrations of OC and EC were 17.4 μg m^{-3} and 4.9 μg m^{-3}, with the range of 2.0–45.4 μg m^{-3} and 0.3–19.8 μg m^{-3}, respectively (see Table 1). The total carbon (TC = OC + EC) accounted for 16.5% of the $PM_{2.5}$ concentration, with OC and EC accounted for 13.1% and 3.4%, respectively, indicating that carbonaceous aerosols were one of the key components of fine particles in Dongshan. In addition, Strong correlations (r) of 0.79 between TC and $PM_{2.5}$ mass concentrations was observed in Dongshan, implying TC and $PM_{2.5}$ have similar sources and formation processes.

3.1.2. Temporal variation of major air pollutants

Fig. 2 shows the time series of concentrations of six gaseous species and carbonaceous aerosols during the period from January 15 to 28, 2015, at Dongshan. A cold front from north has passed through Dongshan and brought a rainfall before January 15. Due to the wet scavenging effect, the concentrations of air pollutants on January 15, 2015 remained at a very low level. Since then, several pollution events were observed with high pollution levels (see yellow circle marks in Fig. 2). The concentrations of OC, EC and CO showed similar trends to $PM_{2.5}$ mass concentrations with a clear accumulating process from January 15 to 26. Based on the variations of air pollutants and transport pattern (see Table 3), the whole period was divided into five different periods with distinct features. In the first period (P1; 08:00 16 January to 08:00 17 January), the mean concentrations of $PM_{2.5}$ and PM_{10} were 82.3 μg m^{-3} and 114.1 μg m^{-3}, respectively. There was a slow but steady increase in $PM_{2.5}$ concentration, similar variations were found for OC, EC, CO and NO_2. In the second period (P2; 09:00 17 January to 08:00 21 January), the mean concentrations of $PM_{2.5}$ and PM_{10} were 48.6 μg m^{-3} and 98.3 μg m^{-3}, respectively, which is relatively low. The CO concentration was also lower than that of P1. However, the O_3, SO_2 and NO_2 concentrations were higher than P1.

In the third period (P3; 09:00 21 January to 05:00 23 January), the mean concentrations of $PM_{2.5}$ and PM_{10} were 75.7 μg m^{-3} and 115.8 μg m^{-3}, respectively, which were 1.5 and 1.2 times as high as that during P2. An obvious haze event was observed in this period. PM, OC and EC concentrations were characterized by a dramatic increase to the highest levels and then a rapid decrease to a low level. $PM_{2.5}$ and PM_{10} concentrations started to increase rapidly from 17:00 21 January reaching their maxima (i.e., 172.9 μg m^{-3} and 285.0 μg m^{-3}) at 20:00 21 January and subsequently decreased rapidly to 49.3 μg m^{-3} and 66.2 μg m^{-3} at 01:00 22 January, respectively. However, this change was not found for other trace gases such as O_3, CO, SO_2 and NO_2. In the fourth period (P4; 06:00 23 January to 23:00 25 January), the mean concentrations of $PM_{2.5}$ and PM_{10} were 86.8 μg m^{-3} and 126.4 μg m^{-3}, respectively, which were 1.8 and 1.3 times of those during P2. In this period, two haze events were observed. All the air pollutants were characterized by two obvious increases at the same time. While in the last period (P5; 00:00 26 January to 13:00 28 January), the mean concentrations of $PM_{2.5}$ and PM_{10} were 45.4 μg m^{-3} and 69.4 μg m^{-3}, respectively. $PM_{2.5}$ and PM_{10} decreased rapidly and remained low followed by the other cold air activity from north passing through Dongshan with clean air masses, resulting in a large scale of precipitation.

3.1.3. Diurnal variation of major air pollutants

The diurnal evolutions of air pollutants and carbonaceous aerosols are illustrated in Fig. 3. The concentrations of all the air pollutants and carbonaceous aerosols maintained high levels in the daytime and low levels in the nighttime, indicating the strong impact of human activities on air quality in Dongshan. O_3 concentrations showed most obvious diurnal variations with the lowest levels at 05:00 in the morning and the highest at 15:00 in the afternoon. As a secondary pollutant, the photochemical production of O_3 is closely related to solar radiation (Latif et al., 2012; Cheung and Wang, 2001). The diurnal variations of $PM_{2.5}$ and PM_{10} showed the bimodal pattern with the first peak appeared at 11:00 at noon and the second peak appeared at 19:00 in the evening. A similar trend was found for NO_2 with the first peak appeared at 9:00 and the second peak appeared at 16:00. The diurnal variation of OC and EC also showed the bimodal pattern with the first peak appeared at 12:00 and 9:00, respectively, and the second peak both appeared at 18:00, which was associated with traffic-related emissions during rush hours. The diurnal variations of CO and SO_2 showed the unimodal pattern with the peak appeared at 12:00 and 11:00 at noon, respectively and the valley both appeared at 23:00 in the evening. CO and SO_2 are emitted directly from sources such as biomass burning, fuel and coal combustion, their concentrations can be affected significantly by the local sources (Yan et al., 2015; Luvsan et al., 2012). Lower concentrations of all the air pollutants except O_3 were observed in the afternoon when the planetary

Table 1
Statistical summary on the $PM_{2.5}$, PM_{10}, SO_2, CO, NO_2, O_3, OC and EC concentrations, the ratios of $PM_{2.5}/PM_{10}$, OC/EC and $TC/PM_{2.5}$ from 15 to 28 January, 2015, at Dongshan site. (The concentrations of $PM_{2.5}$, PM_{10}, SO_2, CO, NO_2 and O_3 were online data with hourly resolution and The OC and EC data were offline data with 3-h resolution.).

	Average	Standard deviation	Maximum	Minimum
$PM_{2.5}$ (μg m^{-3})	61.5	32.2	177.1	2.1
PM_{10} (μg m^{-3})	98.2	46.5	285.0	5.1
O_3 (μg m^{-3})	48.7	28.5	129.7	10.7
CO (mg m^{-3})	1.2	0.6	3.1	0.1
SO_2 (μg m^{-3})	36.7	24.4	186.0	5.4
NO_2 (μg m^{-3})	53.2	28.2	238.8	12.2
$PM_{2.5}/PM_{10}$ (%)	62.8	13.6	93.4	30.0
OC (μg m^{-3})	17.4	8.8	45.4	2.0
EC (μg m^{-3})	4.9	3.3	19.8	0.3
OC/EC	4.2	1.7	12.0	1.8
$TC/PM_{2.5}$ (%)	16.5	6.2	34.5	1.8

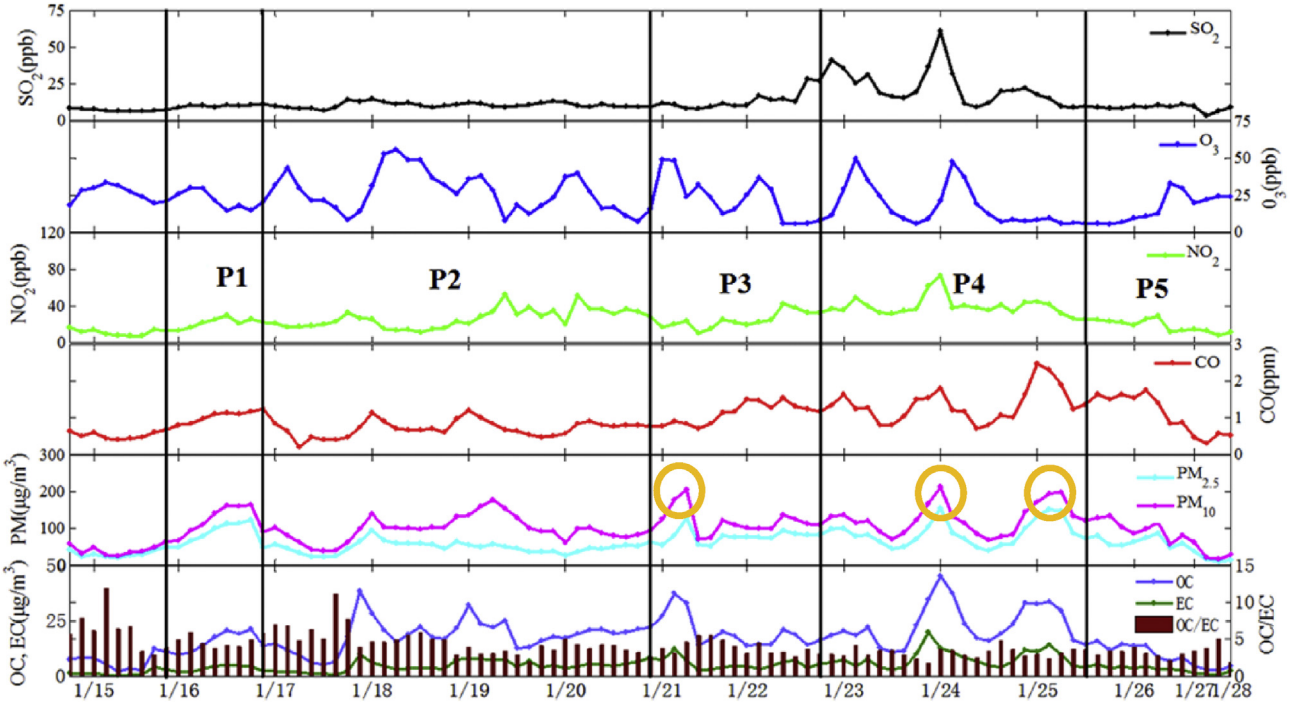

Fig. 2. Time series of concentrations of $PM_{2.5}$, PM_{10}, SO_2, CO, O_3, NO_2, OC, EC and the OC/EC ratios from 15 to 28 January, 2015, at Dongshan site.

boundary layer (PBL) became deeper and wind speed increased (Zhang and Cao, 2015; Wang et al., 2015; Xu et al., 2014).

The PBL height from 15 to 28 January, 2015, at Dongshan was derived from the U.S. National Oceanic and Atmospheric Administration (NOAA) READY archived meteorological GDAS data. Anti-correlation between the PBL and PM concentrations was found during 15–28 January, 2015, in Dongshan. The correlation coefficients between the PBL height and $PM_{2.5}$, PM_{10} concentrations were −0.20 and −0.24 ($P < 0.05$), respectively, indicating the low PBL height contributes to the enhanced accumulation of particulate matter formation.

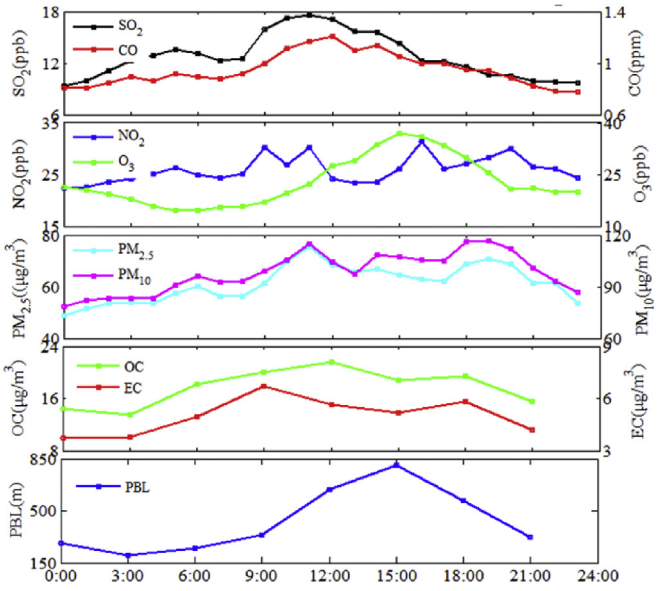

Fig. 3. Diurnal variations of concentrations of $PM_{2.5}$, PM_{10}, SO_2, CO, O_3, NO_2, OC and EC from 15 to 28 January, 2015, at Dongshan site.

3.1.4. Correlation between major air pollutants

Table 2 summarizes the correlation coefficients between major air pollutants and carbonaceous aerosols for the whole period. $PM_{2.5}$ was highest correlated with CO ($r = 0.79$), followed by SO_2 ($r = 0.51$) and NO_2 ($r = 0.51$), reflecting the common sources of these species from fossil fuel combustion. NO_2 are mostly from fossil fuels burning (Lamarque et al., 2010) and CO has a relatively long lifetime in the atmosphere with well-known sources such as fossil fuels or firewood burning and oxidation of hydrocarbons (Yu et al., 2006; Xu et al., 2015). OC and EC had good correlations with $PM_{2.5}$ and PM_{10}, which implied that OC, EC and particulate matters have similar sources and formation processes. OC and EC also had good correlations with NO_2, CO and SO_2, which provided another evidence that vehicle emission and coal combustion may be the dominant sources of OC and EC in $PM_{2.5}$ in Dongshan. Better correlation between EC and NO_2 was found than that between OC and NO_2 or between EC and SO_2, implying the more significant effect of traffic sources on EC emissions. However, negative correlations were found between O_3 and other air pollutants such as $PM_{2.5}$, PM_{10}, NO_2 and CO, which can be attributed to O_3 consumption during the oxidation of NO to NO_2 (Wang et al., 2014b). Moreover, particulate matter in the atmosphere can scatter and absorb light, affecting the visibility and solar radiation transfer, thus results in the decreased photochemical production of O_3 (Yang et al., 2015; Cheung and Wang, 2001).

3.2. Sources of carbonaceous aerosols

Carbonaceous aerosol originates from a variety of emission sources, the relationship between OC and EC and the ratio of OC to EC is an important factor that provides information about the source type of carbonaceous aerosols (Turpin and Huntzicker, 1995; Cao et al., 2007; Ji et al., 2016; Pio et al., 2011). A strong correlation between OC and EC was found in $PM_{2.5}$ with a correlation coefficient of 0.88, indicating that the two species maybe originated from similar emission sources and transport processes. Previous studies

Table 2
Correlations between $PM_{2.5}$, PM_{10}, SO_2, CO, O_3, NO_2, OC and EC from 15 to 28 January at Dongshan site.

	$PM_{2.5}$	PM_{10}	CO	NO_2	SO_2	O_3	OC	EC
$PM_{2.5}$	1							
PM_{10}	0.88[a]	1						
CO	0.79[a]	0.67[a]	1					
NO_2	0.51[a]	0.59[a]	0.48[a]	1				
SO_2	0.51[a]	0.43[a]	0.45[a]	0.59[a]	1			
O_3	−0.23[a]	−0.16[a]	−0.33[a]	−0.37[a]	−0.06	1		
OC	0.69[a]	0.79[a]	0.52[a]	0.62[a]	0.51[a]	0.00	1	
EC	0.66[a]	0.75[a]	0.60[a]	0.70[a]	0.54[a]	−0.17	0.88[a]	1

[a] Correlation is significant at the 0.01 level (2-tailed).

have shown that high OC/EC ratios were related to biomass burning or the formation of SOC whereas low OC/EC ratios were related to fossil-fuel emissions like vehicle exhaust (Schauer et al., 2002; Zhang et al., 2007b). Watson et al. (2001) reported that the OC/EC ratios measured with TOR method for coal combustion, vehicle emission, and biomass burning were 2.7, 1.1 and 9.0, respectively. The OC/EC ratios in Dongshan ranged from 1.8 to 12.0 with a mean value of 4.2, which was comparable with the average ratio of 4.0 reported for 14 Chinese cities (Cao et al., 2007), indicating that vehicle exhaust, coal combustion, biomass burning were the possible sources of carbonaceous species in Dongshan.

The ratio of OC to EC is influenced by many factors, such as the chemical composition of the fuels, the effectiveness of pollution control devices, the sampling environment or analytical methods. Therefore, the application of OC/EC ratios to source identification requires either an assumption that the ambient OC was POC or a way to estimate the SOC.

To better understand the contribution of SOC formation, we used the EC tracer method, which is based on the ratio of OC/EC to estimate SOC. This method assumes that: (1) in contrast with non-volatile organics, the contribution of semi-volatile organic compounds' contribution is relatively small; (2) the composition of primary carbonaceous aerosol emissions and the contribution of each origin remain constant spatially and temporally; and (3) the contribution of non-combustion POC is small or constant (Castro et al., 1999). Such a method has some limitations; for example, SOC will be overestimated when biomass burning occurred with high emission ratio of OC to EC (Pio et al., 2011). Despite of the limitation, EC-tracer method is believed to provide reasonable and semi-quantitative SOC and has still been widely used in many other studies (Chen et al., 2016; Ji et al., 2016; Liu et al., 2016). The equations are as follows:

$$SOC = OC_{total} - OC_{pri} \quad (4)$$

$$OC_{pri} = EC\left(\frac{OC}{EC}\right)_{pri} + N \quad (5)$$

where OC_{pri} is primary organic carbon, and $(OC/EC)_{pri}$ is the ratio for primary sources contributing to the sample OC/EC ratio. N is the contribution of POC from non-combustion sources or sampling artifacts. Castro et al. (1999) reported that $(OC/EC)_{pri}$ could be represented by the observed minimum (OC/EC) ratio. Lim and Turpin (2002) improved this method by taking regression analysis on the 10–20% percentile of the lowest OC/EC ratios to get the $(OC/EC)_{pri}$ and N. In this study, linear regression was adopted based on the lowest 10% of the measured OC/EC values and the slope of 1.83 and intercept of 3.77 was adopted as the $(OC/EC)_{pri}$ and N.

Based on the equations, the averaged estimated SOC concentration for the whole period was 5.7 μg m^{-3}, accounting for 28.4% of the total OC in Dongshan. Fig. 4 shows the SOC/OC and OC/EC ratios during different periods. The average OC/EC ratios from P1 to P5 were 4.3, 4.7, 3.9, 3.1 and 3.3, respectively. The average SOC concentrations from P1 to P5 were 4.8 μg m^{-3}, 6.9 μg m^{-3}, 6.3 μg m^{-3}, 5.5 μg m^{-3} and 2.6 μg m^{-3}, accounting for 29.3%, 32.7%, 29.6%, 22.0% and 9.1% of the total OC, respectively, indicating that SOC formation can be an important component of OC mass in Dongshan. It should be noted that high OC/EC and SOC formation were found during P1, P2 and P3 which might be associated with the long-range and regional air mass transport, which was favorable for OC aging and thus caused high SOC formation. Low OC/EC ratio and SOC formation were found during P4, indicating local emissions during P4, as discussed in the following sections of air mass trajectories clustering and PSCF and CWT analysis. The very low SOC level during P5 might be more affected by the unfavorable meteorological conditions with rain and snow.

3.3. Air mass trajectories clustering

As mentioned above, $PM_{2.5}$ was the main air pollutant in Dongshan. In this work, trajectory clustering approach was applied to identify different transport patterns of $PM_{2.5}$ for different periods at

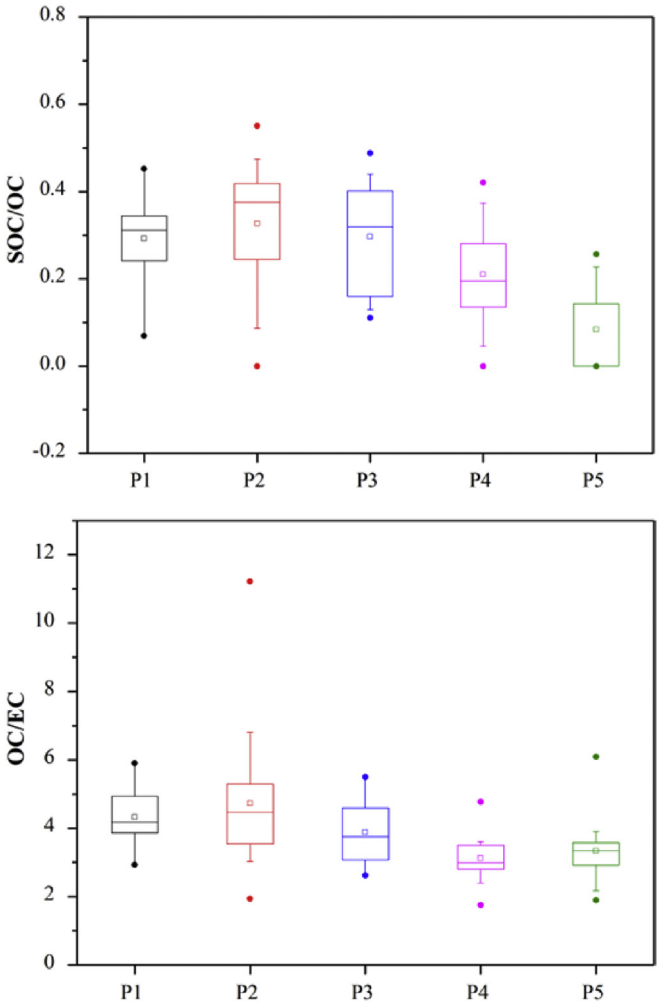

Fig. 4. The SOC/OC (above) and OC/EC (below) ratios during different periods. The central box represents the values from the lower to upper quartile (25th to 75th percentile). The middle line represents the median. The vertical line extends from the 10th percentile to the 90th percentile. The hollow square represents the average value. The dots represent the maximum and minimum values.

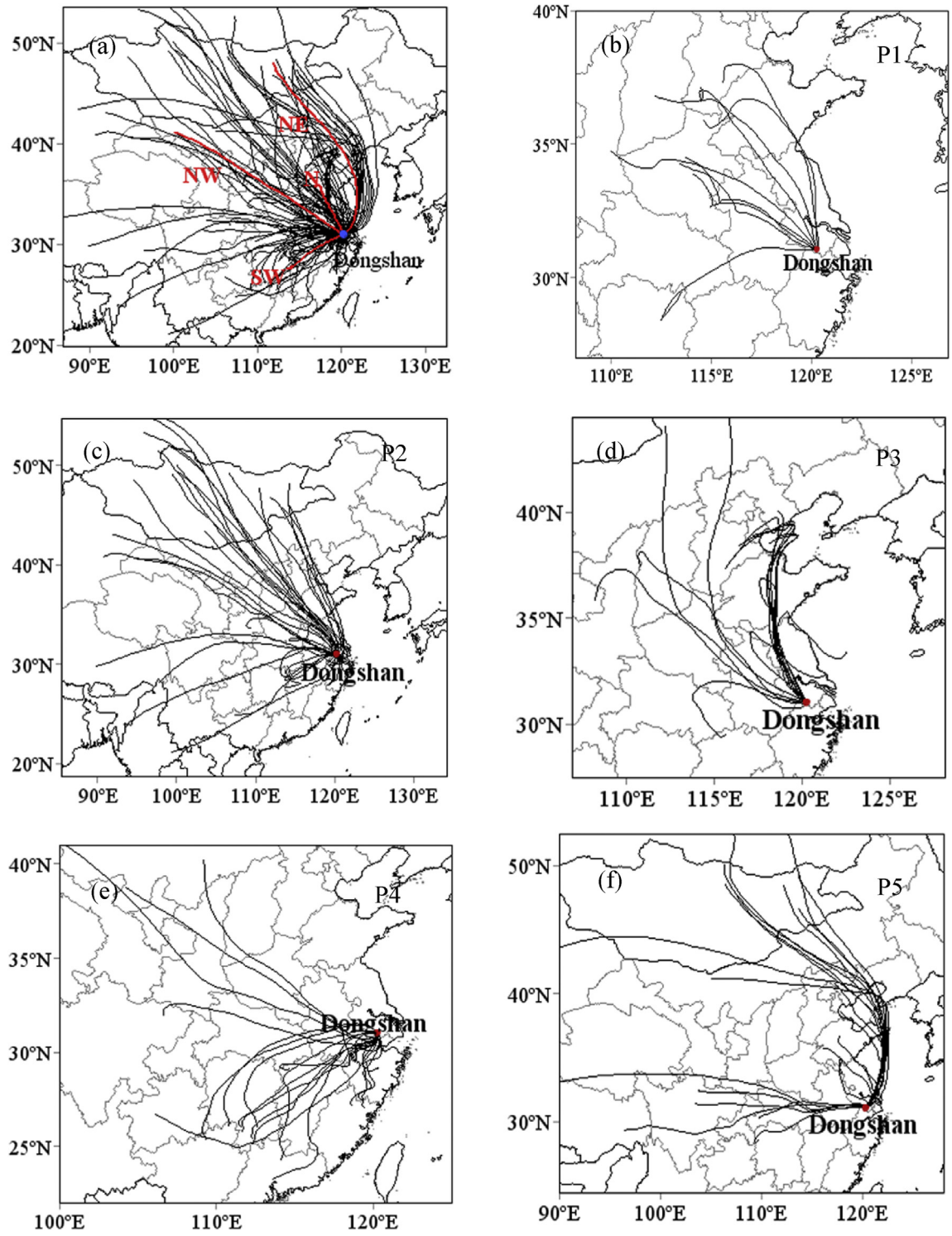

Fig. 5. The 48-h back trajectories at 500 m in Dongshan from 15 to 28 January for (a) the whole period from 15 to 28 January. (b) P1 from January 16 08:00 to January 17 08:00; (c) P2 from January 17 09:00 to January 21 08:00; (d) P3 from January 21 09:00 to January 23 05:00; (e) P4 from January 23 06:00 to January 25 23:00; (f) P5 from January 26 00:00 to January 28 13:00.

Dongshan (Fig. 5). As shown in Fig. 5(a), four clusters for all data during the whole period were calculated: NE (Northeast), N (North), NW (Northwest) and SW (Southwest). The back trajectories for P1 to P5 are shown in Fig. 5(b), (c), (d), (e) and (f), respectively. The percentages of trajectories for each cluster as well as mean $PM_{2.5}$ concentrations and wind speeds during each period (i.e., P1 to P5) are summarized in Table 3. In addition, the transport pattern and the results for polluted cases when $PM_{2.5}$ concentrations exceeding 75 μg m^{-3} (the Class II NAAQS) are also presented in Table 3. For the whole period, the NW cluster was the dominant direction with percentages of 29.5% in total air mass trajectories and the SW, N and NE clusters accounted for 27.7%, 25.9% and 17.0%, respectively.

Table 3
Mean concentrations of $PM_{2.5}$ and percentages of trajectories during the whole period (15–28 January) and during different periods, i.e., P1 (from January 16 08:00 to January 17 08:00), P2 (from January 17 09:00 to January 21 08:00), P3 (from January 21 09:00 to January 23 05:00), P4 (from January 23 06:00 to January 25 23:00), P5 (from January 26 00:00 to January 28 13:00).

	Transport pattern	Direction	Percent (%)	Mean $PM_{2.5}$ ($\mu g\ m^{-3}$)	Polluted Mean $PM_{2.5}$ ($\mu g\ m^{-3}$)	Polluted Percent (%)	Wind Speed ($m\ s^{-1}$)
All data for the whole period		N	25.9 (29)	70.6	94.8	48.3 (14)	3.0
		SW	27.7 (31)	71.0	112.7	32.2 (10)	2.2
		NW	29.5 (33)	57.6	87.6	21.2 (7)	2.5
		NE	17.0 (14)	27.3	0.0	0.0 (0)	2.6
P1 (16/Jan-17/Jan)	Regional transport	NW	55.6 (5)	61.0	85.3	20.0 (1)	2.6
		N	44.4 (4)	108.8	108.8	100.0 (4)	1.6
P2 (18/Jan-20/Jan)	Long-range transport and regional transport	NW	59.4 (19)	47.5	0.0	0.0 (0)	2.5
		SW	40.6 (13)	50.3	84.7	15.4 (2)	2.7
P3 (21/Jan-22/Jan)	Long-range transport	NW	26.7 (4)	68.3	82.3	50.0 (2)	2.9
		N	73.3 (11)	78.4	89.0	63.6 (7)	4.1
P4 (23/Jan-25/Jan)	Regional transport and local sources	SW	100.0 (22)	86.8	111.1	54.5 (12)	2.4
P5 (26/Jan-28/Jan)	Long-range transport	NE	66.7 (14)	35.4	99.9	7.1 (1)	2.5
		NW	33.3 (7)	65.6	77.8	28.3 (2)	2.3

The "Polluted Mean $PM_{2.5}$" represents the mean $PM_{2.5}$ concentrations exceeding 75 $\mu g\ m^{-3}$ (the Class II NAAQS). The "polluted Percent" is calculated on the basis of number of trajectories with $PM_{2.5}$ concentration exceeding 75 $\mu g\ m^{-3}$ divided by the total number of trajectories from each direction. Values in the parentheses are the number of back trajectories.

For P1, regional transport was the main transport pattern. The cluster NW accounted for 55.6% of total air masses trajectories with relatively low $PM_{2.5}$ concentration (i.e., 61.0 $\mu g\ m^{-3}$). The cluster N accounted for 44.4% air masses related to high $PM_{2.5}$ concentration of 108 $\mu g\ m^{-3}$ from Shandong, Jiangsu and the south of Hebei provinces. For P2, Long-range transport was the main transport pattern. The cluster NW accounted for 59.4% air masses which originated from far away Mongolia across Inner Mongolia (China) before reaching at Dongshan and brought relatively clean air with low mean $PM_{2.5}$ concentration of 47.5 $\mu g\ m^{-3}$. The cluster SW accounted for 40.6% also brought relatively clean air from Tibet and Yunnan provinces in the west. It should be noted that 15.4% of trajectories from SW brought polluted air masses with polluted mean $PM_{2.5}$ concentration of 84.7 $\mu g\ m^{-3}$ slightly exceeding the NAAQS, which was associated with regional transport. For P3, the long-range predominant cluster N accounted for 73.3% air masses originating from Tianjin municipality across Bohai Bay, Shandong and Jiangsu provinces with a mean $PM_{2.5}$ concentration of 78.4 $\mu g\ m^{-3}$. The cluster NW accounted for 26.7% of total air masses trajectories with relatively low $PM_{2.5}$ concentration (i.e., 68.3 $\mu g\ m^{-3}$). Due to the aerosol aging in the long-range air mass transport process, the transport patterns during P2 and P3 provided the explanations for the high SOC concentrations during as discussed before. For P4, all trajectories came from the SW cluster and brought high polluted air masses with a mean $PM_{2.5}$ concentration of 86.8 $\mu g\ m^{-3}$ from Jiangxi and Hunan provinces as well as local emissions. For P5, the dominant transport pattern was long-range transport similar with P2. The cluster NE accounted for 66.7% air masses with the lowest mean $PM_{2.5}$ concentration of 35.4 $\mu g\ m^{-3}$, originating from the northeast of China across the Yellow Sea and the East Sea before reaching at Dongshan and brought clean air masses and water vapor from the ocean. The cluster NW accounted for 33.3% and also brought clean air from Tibet and Sichuan provinces to Dongshan.

3.4. PSCF and CWT analysis

Maps were created with PSCF and CWT results to specify the level of PSCF and CWT values in terms of a color bar (Fig. 6). Since the air pollution level remained low during P5 as discussed in previous section 3.3, the PSCF and CWT results for P5 are not considered in this section. The areas with high PSCF values were considered as the potential source areas. The areas with high CWT values were considered to make high potential contributions to the high concentrations at the receptor site. As shown in Fig. 6, there were obvious differences in potential source areas for $PM_{2.5}$ during different period.

For P1 (see Fig. 6(a) and (b)), PSCF and CWT showed the similar results. There were two obvious source areas affecting high $PM_{2.5}$ concentrations at Dongshan. One was mainly located in the northwest of Dongshan such as Xingtai and Handan in Hebei province, Liaocheng in Shandong province, Puyang and Luoyang in Henan province. The other potential area was mainly located in the north nearby within 100 km including high-populated cities such as Suzhou, Wuxi and Changzhou in Jiangsu province corresponding to local emissions. The mean wind speed when the trajectories were mainly from north during P1 was 1.6 $m\ s^{-1}$ (see Table 1), which was lowest during the whole period.

For P2 (see Fig. 6(c) and (d)), PSCF results showed that the potential source areas were mainly located in the west of Dongshan such as Xinyang in the south of Henan province, Fuyang, Hefei, Chizhou in Anhui provinces, Xianning in Hubei province and Nanchang in Jiangxi province. CWT results showed that Fuyang, Liu'an, Ma'anshan in Anhui province may have a great contribution to Dongshan's high $PM_{2.5}$ concentrations.

For P3 (see Fig. 6(e) and (f)), the distributions of PSCF and CWT values showed a major source region from Tianjin municipality across Bohai Bay, Shandong and Jiangsu province due to long-range transport, which brought highly polluted air masses to Dongshan with the highest mean wind speed during the whole period of 4.1 $m\ s^{-1}$ (see Table 1). The sources affecting high $PM_{2.5}$ concentrations at Dongshan were mainly located in Tianjin municipality, Dongying, Rizhao and Linyi in Shandong province, Xuzhou, Suqian, Huai'an, Yangzhou, Changzhou, Wuxi and Suzhou in Jiangsu province.

For P4 (see Fig. 6(g) and (h)), the PSCF results showed that the potential sources affecting high $PM_{2.5}$ concentrations were mainly located in the southwest region of Dongshan. According to the CWT results, strong local source emissions were found during this period. Local sources areas in the southwest nearby within 100 km including high-populated cities such as Wuxi in Jiangsu province, Huzhou in Zhejiang province made great contributions to the high $PM_{2.5}$ concentrations in Dongshan. The strong directly local emissions also explained the lowest SOC formation during P4. The mean wind speed during this period was 2.4 $m\ s^{-1}$ (see Table 1). Meanwhile, areas such as Hangzhou in Zhejiang province, Xuancheng,

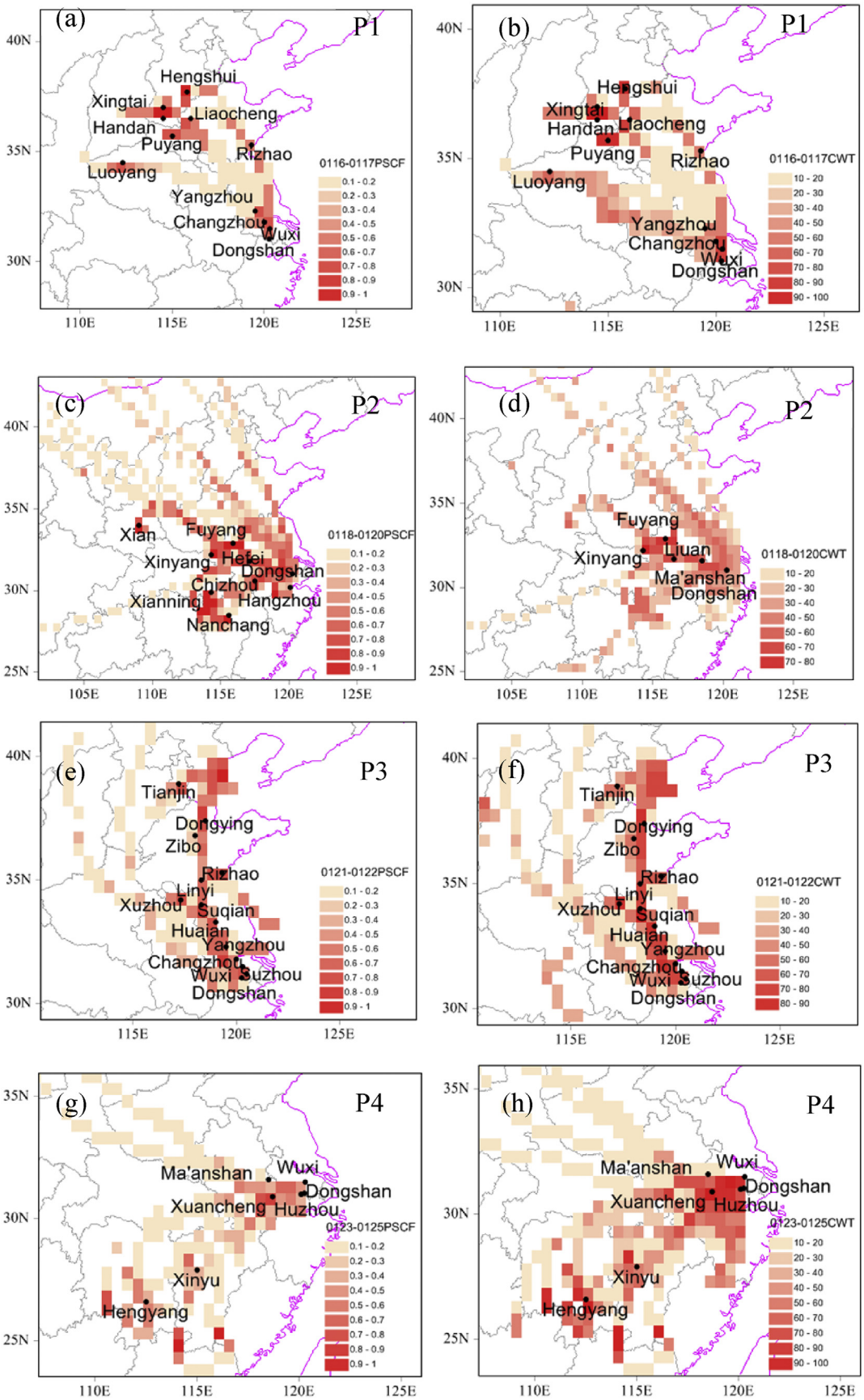

Fig. 6. The PSCF and CWT maps for $PM_{2.5}$ for (a) and (b) P1 from January 16 08:00 to January 17 08:00; (c) and (d) P2 from January 17 09:00 to January 21 08:00; (e) and (f) P3 from January 21 09:00 to January 23 05:00; (g) and (h) P4 from January 23 06:00 to January 25 23:00.

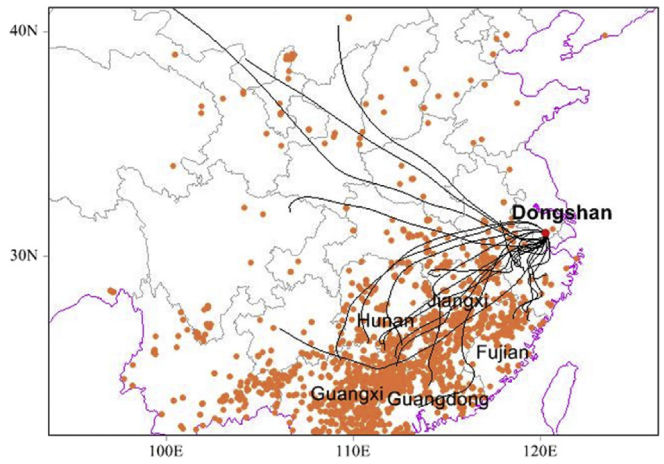

Fig. 7. The 48-h backward trajectories from January 23 to 25, 2015 plotted on the fire map from January 21 to 25, 2015 obtained from the Fire Information for Resource Management System (FIRMS) derived from the Moderate Resolution Imaging Spectroradiometer (MODIS).

Ma'anshan in Anhui province, Hengyang in Hunan province and Xinyu in Jiangxi province also had a great contribution to Dongshan's high $PM_{2.5}$ concentrations. It is of interest to note that during this period, large numbers of fire pots were monitored in the areas such as Jiangxi, Hunan, Guangdong and Fujian provinces (see Fig. 7). The back trajectories analysis showed that the air masses during this period passed through these areas, indicating a strong impact of biomass burning emissions on the $PM_{2.5}$ concentrations and the other air pollutants. Further chemical and carbon isotope analysis are needed to verify it (Cao et al., 2015).

In this study, it was found that $PM_{2.5}$ concentrations in Dongshan under different wind speed conditions have shown different source features. Under high wind speed conditions, strong long-range transport was found (i.e., P3), while under low wind speed conditions strong local emissions were found (i.e., P1 and P4). Both of the two conditions could lead to high $PM_{2.5}$ concentrations.

4. Conclusions

In this study, the characteristics and geographical origins of the major air pollutants ($PM_{2.5}$, PM_{10}, CO, SO_2, NO_2 and O_3) and carbonaceous aerosols were analyzed during 15–28 January, 2015, at Dongshan, a rural site in the Yangtze River Delta of China. $PM_{2.5}$ on average contributed 63% to PM_{10} for the whole period, indicating the significant fine particulate matter pollution in Dongshan. TC accounted for 16.5% of $PM_{2.5}$ mass. SOC accounted for nearly one third of OC on average, highlighting the significance of SOC formation in wintertime haze pollution. Based on the variations of air pollutants, we separated the whole period into five sub-periods: P1 (08:00 16 January to 08:0017 January), P2 (09:0017 January to 08:00 21 January), P3 (09:00 21 January to 05:00 23 January), P4 (06:00 23 January to 23:00 25 January) and P5 (00:00 26 January to 13:00 28 January). The mean $PM_{2.5}$ concentrations for P1 to P5 were 82.3 μg m^{-3}, 48.6 μg m^{-3}, 75.7 μg m^{-3}, 86.8 μg m^{-3} and 45.4 μg m^{-3}, respectively. The NOAA HYAPLIT model and the PSCF and CWT analysis showed that different pollution periods had distinct different transport patterns. Lower $PM_{2.5}$ concentrations during clean periods of P2 and P5 were associated with long-range transported air masses originated from remote regions such as Mongolia, Inner Mongolia and oceanic areas (i.e., the Yellow Sea and the East Sea). During haze periods, regional transport during P1 and P3 and strong local emissions during P4 both made great contributions to high $PM_{2.5}$ concentrations in Dongshan. Significant air masses transport from industrial cities in the north of Dongshan such as Hengshui, Xingtai, Handan in Hebei province, Liaocheng, Linyi, Dongying in Shandong province, Luoyang in Henan province to Dongshan were found. In addition, polluted air masses from high-populated cities in the nearby provinces such as Suzhou, Wuxi, Changzhou in Jiangsu province, Hangzhou, Huzhou in Zhejiang province, Hefei in Anhui province and Nanchang in Jiangxi province also made a great contribution to the extreme haze episodes in Dongshan. Biomass burning in the southwest of Dongshan such as Jiangxi, Hunan, Guangdong and Fujian might have also significantly decreased air quality in Dongshan, which was supported by MODIS fire spots and receptor models. It should be noted that strong SOC formation was found under long-range transport pattern, which was favorable for aerosol aging whereas low SOC formation was found when there was strong local emission. $PM_{2.5}$ concentrations in Dongshan under different wind speed conditions showed different source features. In addition to local emissions, high $PM_{2.5}$ concentrations at Dongshan were affected by either regional or long-range transport, which were characterized by relatively low and high wind speeds, respectively. The correlation analysis among the air pollutants and carbonaceous aerosols revealed the importance of fossil fuel combustion and vehicle emission in Dongshan. To improve the air quality in Dongshan, it is necessary to implement the source emissions control strategies for all the industrial areas locally and regionally, especially the industrial provinces such as Shandong and Hebei provinces and the YRD. It is worth noting that our study did not provide quantitative analysis on the emission sources of air pollutants, further chemical and physical analysis, for instance, Positive Matrix Factorization (PMF), a source-receptor model analysis are needed to identify more detailed emission source information (Bari and Kindzierski, 2017 . Begum and Hopke, 2013; Sahu et al., 2011).

Acknowledgments

We acknowledge the financial support by the Natural Science Foundation for Young Scientists of Jiangsu Province, China (BK20150895), and the National Natural Science Foundation of China (41603104 and 91644103), and the Startup Foundation for Introducing Talent of NUIST (No. 2015r023 and 2015r019).

References

Adame, J.A., Notario, A., Villanueva, F., Albaladejo, J., 2012. Application of cluster analysis to surface ozone, NO_2 and SO_2 daily patterns in an industrial area in Central-Southern Spain measured with a DOAS system. Sci. Total Environ. 429, 1–3.

Ashbaugh, L.L., Malm, W.C., Sadeh, W.Z., 1985. A residence time probability analysis of sulfur concentrations at grand Canyon National Park. Atmos. Environ. 19, 1263–1270.

Bari, M.A., Kindzierski, W.B., 2017. Characteristics of air quality and sources affecting fine particulate matter ($PM_{2.5}$) levels in the City of Red Deer, Canada. Environ. Pollut. 221, 367–376.

Begum, B.A., Hopke, P.K., 2013. Identification of haze-creating sources from fine particulate matter in Dhaka aerosol using carbon fractions. J. Air Waste Manage. Assoc. 63, 1046–1057.

Bergin, M.S., West, J.J., Keating, T.J., Russell, A.G., 2005. Regional atmospheric pollution and transboundary air quality management. Environ. Res. 30, 1–37.

Cao, F., Zhang, S.C., Kawamura, K., Zhang, Y.L., 2015. Inorganic markers, carbonaceous components and stable carbon isotope from biomass burning aerosols in Northeast China. Sci. Total Environ. 24, 671–682.

Cao, J.J., Lee, S.C., Chow, J.C., Watson, J.G., Ho, K.F., Zhang, R.J., Shen, Z.X., Chen, G.C., Kang, Y.M., Zou, S.C., Zhang, L.Z., Qi, S.H., Dai, M.H., Cheng, Y., Hu, K., 2007. Spatial and seasonal distributions of carbonaceous aerosols over China. J. Geophys. Res. Atmos. D112, 22–11.

Cao, J.J., Shen, Z.X., Chow, J.C., John, G., Watson, J.G., Lee, S.C., Tie, X.X., Ho, K.F., Wang, G.H., Han, Y.M., 2012. Winter and summer $PM_{2.5}$ chemical compositions in fourteen Chinese cities. J. Air Waste Manage. Assoc. 62, 1214–1226.

Cao, J.J., Wu, F., Chow, J.C., Lee, S.C., 2005. Characterization and source apportionment of atmospheric organic and elemental carbon during fall and

winter of 2003 in Xi'an, China. Atmos. Chem. Phys. 5, 3127–3137.
Cao, J.J., Zhu, C.S., Tie, X.X., Geng, F.H., Xu, H.M., Ho, S.S.H., Wang, G.H., Han, Y.M., Ho, K.F., 2013. Characteristics and sources of carbonaceous aerosols from Shanghai, China. Atmos. Chem. Phys. 13, 803–817.
Castro, L.M., Pio, C.A., Harrison, R.M., Smith, D.J.T., 1999. Carbonaceous aerosol in urban and rural European atmospheres: estimation of secondary organic carbon concentrations. Atmos. Environ. 33, 2771–2781.
Chan, C.K., Yao, X., 2008. Air pollution in mega cities in China. Atmos. Environ. 42, 1–42.
Chang, L.T., Tsai, J.H., Lin, J.M., Huang, Y.S., Chiang, H.L., 2011. Particulate matter and gaseous pollutants during a tropical storm and air pollution episode in Southern Taiwan. Atmos. Res. 99, 67–79.
Chen, D., Cui, H., Zhao, Y., Yin, L., Lu, Y., Wang, Q., 2016. A two-year study of carbonaceous aerosols in ambient $PM_{2.5}$, at a regional background site for western Yangtze River Delta. China. Atmos. Res. 183, 351–361.
Chen, R., Peng, R.D., Meng, X., Zhou, Z., Chen, B., Kan, H., 2013. Seasonal variation in the acute effect of particulate air pollution on mortality in the China Air Pollution and Health Effects Study (CAPES). Sci. Total Environ. 450–451, 259–265.
Cheung, V.T.F., Wang, T., 2001. Observational study of ozone pollution at a rural site in the Yangtze Delta of China. Atmos. Environ. 35, 4947–4958.
Draxler, R.R., Hess, G.D., 1998. An overview of the HYSPLIT_4 modeling system of trajectories, dispersion, and deposition. Aust. Meteor. Mag. 47, 295–308.
GDAS (Global Data Assimilation System), 2007. http://ftp://arlftp.arlhq.noaa.gov/pub/archives/gdas1, (Accessed in January 2015).
Guo, S., Hu, M., Zamora, M.L., Peng, J., Shang, D., Zheng, J., Du, Z.F., Wu, Z.J., Shao, M., Zeng, L.M., Molina, M.J., Zhang, R.Y., 2014. Elucidating severe urban haze formation in China. Proc. Natl. Acad. Sci. U. S. A. 111, 17373–17378.
Hoh, E., Hites, R.A., 2004. Sources of toxaphene and other organochlorine pesticides in North America as determined by air measurements and potential source contribution function analyses. Environ. Sci. Technol. 38, 4187–4194.
Hsu, Y.K., Holsen, T.M., Hopke, P.K., 2003. Comparison of hybrid receptor models to locate PCB sources in Chicago. Atmos. Environ. 37, 545–562.
Huang, R.J., Zhang, Y., Bozzetti, C., Ho, K.F., Cao, J.J., Han, Y.M., Daellenbach, K.R., Slowik, J.G., Platt, S.M., Canonaco, F., Zotter, P., Wolf, R., Pieber, S.M., Bruns, E.A., Ciarelli, G., Piazzalunga, A., Schwikowski, M., Abbaszade, G., Jürgen, S.K., Zimmermann, R., An, Z.S., Szidat, S., Baltensperger, U., Haddad, I.E., Prévôt, A.S.H., 2014. High secondary aerosol contribution to particulate pollution during haze events in China. Nature 514, 218–222.
Jacobson, M.Z., 2001. Strong radiative heating due to the mixing state of black carbon in atmospheric aerosols. Nature 409, 695–697.
Ji, D., Zhang, J., He, J., Wang, X., Pang, B., Liu, Z., Wang, L., Wang, Y., 2016. Characteristics of atmospheric organic and elemental carbon aerosols in urban Beijing, China. Atmos. Environ. 125, 293–306.
Kaiser, D.P., Yun, Q., 2002. Decreasing trends in sunshine duration over China for 1954–1998: indication of increased haze pollution? Geophys. Res. Lett. 29, 1–4.
Karaca, F., Anil, I., Alagha, O., 2009. Long-range potential source contributions of episodic aerosol events to PM_{10}, profile of a megacity. Atmos. Environ. 43, 5713–5722.
Kim, Y.J., Woo, J.H., Ma, Y.I., Kim, S., Nam, J.S., Sung, H., Choi, K.C., Seo, J., Kim, J.S., Kang, C.H., Lee, G., Ro, C.U., Chang, D., Sunwoo, Y., 2009. Chemical characteristics of long-range transport aerosol at background sites in Korea. Atmos. Environ. 43, 5556–5566.
Lamarque, J.F., Bond, T.C., Eyring, V., Granier, C., 2010. Historical (1850–2000) gridded anthropogenic and biomass burning emissions of reactive gases and aerosols: methodology and application. Atmos. Chem. Phys. 10, 7017–7039.
Latif, M.T., Huey, L.S., Juneng, L., 2012. Variations of surface ozone concentration across the Klang Valley, Malaysia. Atmos. Environ. 61, 434–445.
Lim, H.J., Turpin, B.J., 2002. Origins of primary and secondary organic aerosol in atlanta: results of time-resolved measurements during the Atlanta supersite experiment. Environ. Sci. Technol. 36, 4489–4496.
Liu, B., Bi, X., Feng, Y., Dai, Q., Xiao, Z., Li, L., Wu, J., Yuan, J., Zhang, Y.F., 2016. Fine carbonaceous aerosol characteristics at a megacity during the Chinese Spring Festival as given by OC/EC online measurements. Atmos. Res. 181, 20–28.
Luvsan, M.E., Shie, R.H., Purevdorj, T., Badarch, L., Baldorj, B., Chan, C.C., 2012. The influence of emission sources and meteorological conditions on SO_2, pollution in Mongolia. Atmos. Environ. 61, 542–549.
Mcconnell, J.R., Edwards, R., Kok, G.L., Flanner, M.G., Zender, C.S., Saltzman, E.S., Banta, J.R., Pasteris, D.R., Carter, M.M., Kahl, J.D.W., 2007. 20th-century industrial black carbon emissions altered arctic climate forcing. Science 317, 1381–1384.
MEP (Chinese Ministry of Environmental Protection), 2013a. Technical Specifications for Installation and Acceptance of Ambient Air Quality Continuous Automated Monitoring System for $PM_{2.5}$ and PM_{10}. http://kjs.mep.gov.cn/hjbhbz/bzwb/dqhjbh/jcgfffbz/201308/W020130802492823718666.pdf (Accessed in August 2015).
MEP (Chinese Ministry of Environmental Protection), 2013b. Technical Specifications for Installation and Acceptance of Ambient Air Quality Continuous Automated Monitoring System for SO_2, NO_2, O_3 and CO. http://www.es.org.cn/download/2013/7-12/2627-1.pdf (Accessed in August 2015).
NOAA/ARL, 2007. NOAA ARL HYSPLIT (HYbrid single-particle Lagrangian integrated trajectory) model. Available at: http://gcmd.nasa.gov/records/NOAA-HYSPLIT.html.
Pio, C., Cerqueira, M., Harrison, R.M., Nunes, T., Mirante, F., Alves, C., Oliveira, C., Sanchez de la Campa, A., Artíñano, B., Matos, M., 2011. OC/EC ratio observations in Europe: Re-thinking the approach for apportionment between primary and secondary organic carbon. Atmos. Environ. 45, 6121–6132.
Ramanathan, V., Ramana, M.V., Roberts, G., Kim, D., Corrigan, C., Chung, C., Winker, D., 2007. Warming trends in Asia amplified by brown cloud solar absorption. Nature 448, 575–578.
Sadyś, M., Skjøth, C.A., Kennedy, R., 2014. Back-trajectories show export of airborne fungal spores (Ganoderma, sp.) from forests to agricultural and urban areas in England. Atmos. Environ. 84, 88–99.
Sahu, M., Hu, S., Ryan, P.H., Le Masters, G., Grinshpun, S.A., Chow, J.C., Biswas, P., 2011. Chemical compositions and source identification of $PM_{2.5}$ aerosols for estimation of a diesel source surrogate. Sci. Total Environ. 409, 2642–2651.
Schauer, J.J., Kleeman, M.J., Cass, G.R., Simoneit, B.R.T., 2002. Measurement of emissions from air pollution sources, 5. C1–C32 organic compounds from gasoline-powered motor vehicles. Environ. Sci. Technol. 3, 1169–1180.
Tan, J., Duan, J., Kebin, H.E., Yuanliang, M.A., Duan, F., Chen, Y., Fu, J.M., 2009. Chemical characteristics of $PM_{2.5}$ during a typical haze episode in Guangzhou. J. Environ. Sci. 21, 774–781.
Turpin, B.J., Huntzicker, J.J., 1995. Identification of secondary organic aerosol episodes and quantitation of primary and secondary organic aerosol concentrations during SCAQS. Atmos. Environ. 29, 3527–3544.
Wang, F., Chen, D.S., Cheng, S.Y., Li, J.B., Li, M.J., Ren, Z.H., 2010. Identification of regional atmospheric PM_{10}, transport pathways using HYSPLIT, MM5-CMAQ and synoptic pressure pattern analysis. Environ. Model. Softw. 25, 927–934.
Wang, H., 2015. Chemical composition and light extinction contribution of $PM_{2.5}$ in urban Beijing for a 1-year period. Aerosol Air Qual. Res. 15, 2200–2211.
Wang, M., Cao, C., Li, G., Singh, R.P., 2015. Analysis of a severe prolonged regional haze episode in the Yangtze River Delta, China. Atmos. Environ. 102, 112–121.
Wang, P., Cao, J.J., Shen, Z.X., Han, Y.M., Lee, S.C., Huang, Y., Zhu, C.S., Wang, Q.Y., Xu, H.M., Huang, L.J., 2014a. Spatial and seasonal variations of $PM_{2.5}$, mass and species during 2010 in Xi'an, China. Sci. Total Environ. 508 (C), 477–487.
Wang, Y., Qi, Y., Hu, J., Zhang, H., 2014b. Spatial and temporal variations of six criteria air pollutants in 31 provincial capital cities in China during 2013–2014. Environ. Int. 73, 413–422.
Wang, Y.Q., Zhang, X.Y., Draxler, R.R., 2009. Trajstat: GIS-based software that uses various trajectory statistical analysis methods to identify potential sources from long-term air pollution measurement data. Environ. Model. Softw. 24, 938–939.
Wang, Y.S., Yao, L., Wang, L.L., Liu, Z.R., Ji, D.S., Tang, G.Q., Zhang, J.K., Sun, Y., Hu, B., Xin, J.Y., 2014c. Mechanism for the formation of the January 2013 heavy haze pollution episode over central and eastern China. Sci. China Earth. Sci. 57, 14–25.
Watson, J.G., Chow, J.C., Houck, J.E., 2001. $PM_{2.5}$ chemical source profiles for vehicle exhaust, vegetative burning, geological material, and coal burning in northwestern Colorado during 1995. Chemosphere 43, 1141–1151.
Xu, J., Yan, F., Xie, Y., Wang, F., Wu, J., Fu, Q., 2015. Impact of meteorological conditions on a nine-day particulate matter pollution event observed in December 2013, Shanghai. China. Particuol. 20, 69–79.
Xu, W.Y., Zhao, C.S., Ran, L., Lin, W.L., Yan, P., Xu, X.B., 2014. SO_2 noontime-peak phenomenon in the North China Plain. Atmos. Chem. Phys. 14, 7757–7768.
Xu, X., Akhtar, U.S., 2010. Identification of potential regional sources of atmospheric total gaseous mercury in Windsor, Ontario, Canada using hybrid receptor modeling. Atmos. Chem. Phys. 10, 7073–7083.
Yan, R., Yu, S., Zhang, Q., Li, P., Wang, S., Chen, B., Liu, W.P., 2015. A heavy haze episode in Beijing in February of 2014: characteristics, origins and implications. Atmos. Pollut. Res. 6, 867–876.
Yang, F., Tan, J., Zhao, Q., Du, Z., He, K., Ma, Y., Duan, F., Chen, G., Zhao, Q., 2011. Characteristics of $PM_{2.5}$ speciation in representative megacities and across China. Atmos. Chem. Phys. 11, 5207–5219.
Yang, H., Yu, J.Z., Ho, S.S.H., Xu, J., Wu, W.S., Wan, C.H., Wang, X.D., Wang, X.R., Wang, L.S., 2005. The chemical composition of inorganic and carbonaceous materials in $PM_{2.5}$, in Nanjing, China. Atmos. Environ. 39, 3735–3749.
Yang, Y., Liu, X., Qu, Y., Wang, J., An, J., Zhang, Y., Zhang, F., 2015. Formation mechanism of continuous extreme haze episodes in the megacity Beijing, China, in January 2013. Atmos. Res. 155, 192–203.
Yu, S., Saxena, V.K., Zhao, Z., 2001. A comparison of signals of regional aerosol-induced forcing in eastern China and the southeastern United States. Geophys. Res. Lett. 28, 713–716.
Yu, S., Mathur, R., Kang, D., Schere, K., Eder, B., Pleim, J., 2006. Performance and diagnostic evaluation of ozone predictions by the eta-community multiscale air quality forecast system during the 2002 New England air quality study. J. Air Waste Manage. Assoc. 56, 1459–1471.
Yu, S., Mathur, R., Schere, K., Kang, D., Pleim, J., Otte, T.L., 2007. A detailed evaluation of the Eta-CMAQ forecast model performance for O_3, its related precursors, and meteorological parameters during the 2004 ICARTT study. J. Geophys. Res. Atmos. 112, 185–194.
Yu, S., Rohit, M., Kenneth, S., Kang, D., Jonathan, P., Jeffrey, Y., 2008. Evaluation of real-time $PM_{2.5}$ forecasts and process analysis for $PM_{2.5}$ formation over the eastern United States using the Eta-CMAQ forecast model during the 2004 ICARTT study. J. Geophys. Res. Atmos. 113, 304–312.
Yu, S., Zender, C.S., Saxena, V.K., 2010. Direct radiative forcing and atmospheric absorption by boundary layer aerosols in the southeastern US: model estimates on the basis of new observations. Atmos. Environ. 35, 3967–3977.
Yu, S., Zhang, Y., 2011. An examination of the effects of aerosol chemical composition and size on radiative properties of multi-component aerosols. Atmos. Clim. Sci. 01, 19–32.

Yu, S., Alapaty, K., Mathur, R., Pleim, J., Zhang, Y., Nolte, C., Eder, B., Foley, K., 2013. Attribution of the United States "warming hole": aerosol indirect effect and precipitable water vapor. Sci. Rep. 4, 6929–6929.
Yu, S., 2014. Water spray geoengineering to clean air pollution for mitigating haze in China's cities. Environ. Chem. Lett. 12, 109–116.
Yu, S., Zhang, Q., Yan, R., Wang, S., Li, P., Chen, B., Liu, W.P., Zhang, X.Y., 2014. Origin of air pollution during a weekly heavy haze episode in Hangzhou, China. Environ. Chem. Lett. 12, 543–550.
Zeng, Y., Hopke, P.K., 1989. A study of the sources of acid precipitation in Ontario, Canada. Atmos. Environ. 23, 1499–1509.
Zhang, F., Cheng, H.R., Wang, Z.W., Lv, X.P., Zhu, Z.M., Zhang, G., Wang, X.M., 2014. Fine particles ($PM_{2.5}$) at a CAWNET background site in central China: chemical compositions, seasonal variations and regional pollution events. Atmos. Environ. 86, 193–202.
Zhang, H., Wang, Y., Hu, J., Ying, Q., Hu, X.M., 2015a. Relationships between meteorological parameters and criteria air pollutants in three megacities in China. Environ. Res. 140, 242–254.
Zhang, Q.Y., Yan, R.C., Fan, J.W., Yu, S.C., Yang, W.D., Li, P.F., Wang, S., Chen, B.X., Liu, W.P., Zhang, X.Y., 2015b. A heavy haze episode in shanghai in December of 2013: characteristics, origins and implications. Aerosol Air Qual. Res. 15, 1881–1893.
Zhang, Y.L., Cao, F., 2015. Fine particulate matter ($PM_{2.5}$) in China at a city level. Sci. Rep. 5, 14884.
Zhang, Y.L., Huang, R.J., El Haddad, I., Ho, K.F., Cao, J.J., Han, Y., Zotter, P., Bozzetti, C., Daellenbach, K.R., Canonaco, F., Slowik, J.G., Salazar, G., Schwikowski, M., Schnelle-Kreis, J., Abbaszade, G., Zimmermann, R., Baltensperger, U., Prévôt, A.S.H., Szidat, S., 2015c. Fossil vs. non-fossil sources of fine carbonaceous aerosols in four Chinese cities during the extreme winter haze episode of 2013. Atmos. Chem. Phys. 15, 1299–1312.
Zhang, R.J., Cao, J.J., Lee, S.C., Shen, Z.X., Ho, K.F., 2007a. Carbonaceous aerosols in PM_{10} and pollution gases in winter in Beijing. J. Environ. Sci. 19, 564–571.
Zhang, Y.L., Schnellekreis, J., Abbaszade, G., Zimmermann, R., Zotter, P., Shen, R., Schafer, K., Shao, L., Prévôt, A.S.H., Szidat, S., 2015d. Source apportionment of elemental carbon in Beijing, China: insights from radiocarbon and organic marker measurements. Environ. Sci. Technol. 49, 8408–8415.
Zhang, Y.X., Shao, M., Zhang, Y.H., Zeng, L.M., He, L.Y., Zhu, B., Wei, Y.J., Zhu, X.L., 2007b. Source profiles of particulate organic matters emitted from cereal straw burnings. J. Environ. Sci. 19, 167–175.